Open access • Journal Article • DOI:10.1063/1.4775592

14N overtone NMR spectra under magic angle spinning: experiments and numerically exact simulations. — Source link

Luke A. O'Dell, Andreas Brinkmann

Institutions: National Research Council

Published on: 11 Feb 2013 - Journal of Chemical Physics (American Institute of Physics)

Topics: Magic angle spinning, Magic angle, Solid-state nuclear magnetic resonance and Overtone

14N overtone NMR spectra under magic angle spinning: Experiments and numerically exact simulations

Luke A. O'Dell and Andreas Brinkmann

Citation: J. Chem. Phys. **138**, 064201 (2013); doi: 10.1063/1.4775592
View online: http://dx.doi.org/10.1063/1.4775592
View Table of Contents: http://jcp.aip.org/resource/1/JCPSA6/v138/i6
Published by the AIP Publishing LLC.

THE JOURNAL OF CHEMICAL PHYSICS **138**, 064201 (2013)

^{14}N overtone NMR spectra under magic angle spinning: Experiments and numerically exact simulations

Luke A. O'Dell[a] and Andreas Brinkmann[b]
Measurement Science and Standards, National Research Council Canada, 1200 Montreal Road, M40, Ottawa, Ontario K1A 0R6, Canada

(Received 5 October 2012; accepted 26 December 2012; published online 11 February 2013)

It was recently shown that high resolution ^{14}N overtone NMR spectra can be obtained directly under magic angle spinning (MAS) conditions [L. A. O'Dell and C. I. Ratcliffe, Chem. Phys. Lett. **514**, 168 (2011)]. Preliminary experimental results showed narrowed powder pattern widths, a frequency shift that is dependent on the MAS rate, and an apparent absence of spinning sidebands, observations which appeared to be inconsistent with previous theoretical treatments. Herein, we reproduce these effects using numerically exact simulations that take into account the full nuclear spin Hamiltonian. Under sample spinning, the ^{14}N overtone signal is split into five (0, ±1, ±2) overtone sidebands separated by the spinning frequency. For a powder sample spinning at the magic angle, the $+2\omega_r$ sideband is dominant while the others show significantly lower signal intensities. The resultant MAS powder patterns show characteristic quadrupolar lineshapes from which the ^{14}N quadrupolar parameters and isotropic chemical shift can be determined. Spinning the sample at other angles is shown to alter both the shapes and relative intensities of the five overtone sidebands, with MAS providing the benefit of averaging dipolar couplings and shielding anisotropy. To demonstrate the advantages of this experimental approach, we present the ^{14}N overtone MAS spectrum obtained from L-histidine, in which powder patterns from all three nitrogen sites are clearly resolved. [http://dx.doi.org/10.1063/1.4775592]

I. INTRODUCTION

Nitrogen is one of nature's most abundant elements, but solid-state NMR of nitrogen is difficult due to the unfavorable properties of the two magnetic isotopes, ^{14}N and ^{15}N. The latter is a spin-1/2 nucleus that can, in principle, provide high resolution spectra with narrow linewidths. Unfortunately, it is also very insensitive due to its low natural abundance (0.4%) and low gyromagnetic ratio, and therefore isotopically enriched samples and/or cross-polarization methods are typically required for signal enhancement in solid-state NMR experiments. Despite ^{14}N being generally far more difficult to study, its high natural abundance (99.6%) combined with its potential to provide additional structural information via the quadrupolar interaction has spurred much effort to develop new experimental techniques for this nucleus.[1,2]

The difficulty of ^{14}N solid-state NMR arises from the combination of its quadrupole moment (20.4 mbarn = 2.04 fm^2) and small integer spin number ($I = 1$), which results in large perturbations to the $\Delta m = 1$ (fundamental) Zeeman transitions due to the first-order quadrupolar interaction (typically on the order of several MHz). The dispersion of these transitions over such wide frequency ranges precludes the use of standard solid-state NMR methods, requiring specialized experimental approaches in order to excite and observe the spectra (e.g., broadband magic angle spinning (MAS),[3] piecewise acquisition,[4] or frequency-swept excitation pulses[5]). Recently, two-dimensional methods in which the ^{14}N signal is observed indirectly via a more amenable nucleus such as ^{1}H have gained attention, and are an extremely promising method for probing this isotope.[2] Herein, we consider overtone NMR spectroscopy,[6–8] an alternative approach by which high-resolution ^{14}N NMR spectra can be obtained directly from powder samples.

Bloom and LeGros were the first authors to note that the $\Delta m = 2$, or "overtone," transition is weakly allowed when the magnitudes of the quadrupolar and Zeeman interactions are comparable, and can therefore be excited and observed directly.[6] The primary advantage of this transition is the absence of the first-order quadrupolar interaction that makes the fundamental transitions so difficult to study. The overtone transition is affected only by the second-order quadrupolar interaction and shielding anisotropy, both of which are generally on the order of kHz for the ^{14}N nucleus. Tycko and Opella obtained the first ^{14}N overtone NMR spectra from powder samples[7,8] and demonstrated the advantages of this approach in terms of the significantly reduced spectral range. Unfortunately, this method has failed to become routine due to several quite severe complications, the most important of which stem from the atypical nutation behavior exhibited by the overtone magnetization. Not only are overtone nutation rates very slow compared to the fundamental transitions, requiring long excitation pulses with correspondingly narrow excitation bandwidths, but the rates are also dependent on the strength of the quadrupolar interaction. Refocusing the overtone signal to form a spin-echo is therefore very challenging,

[a]Present address: Institute for Frontier Materials, Deakin University, Waurn Ponds Campus, Geelong, Victoria 3220, Australia.
[b]Author to whom correspondence should be addressed. Electronic mail: Andreas.Brinkmann@nrc-cnrc.gc.ca.

particularly for samples with multiple nitrogen environments. Single-pulse excitation is far more straightforward, but in this case the pre-acquisition delay (i.e., the experimental dead-time between the excitation pulse and signal acquisition) can cause severe lineshape distortions and signal loss, particularly for broader powder patterns.

Recently, the first experimental ^{14}N overtone NMR spectra obtained under MAS were reported.[9] MAS involves spinning the powder sample rapidly about an axis oriented at 54.7° relative to the magnetic field, a method routinely used in solid-state NMR to average or partially average the effects of anisotropic interactions such as the shielding anisotropy, quadrupolar interaction, or dipolar coupling. It was shown that under MAS, ^{14}N overtone powder patterns were significantly narrowed, mitigating the effects of the dead-time and allowing a spectrum to be obtained from the dipeptide L-valyl-L-alanine in which peaks from the two nitrogen sites were well-resolved. Broadband, frequency-swept excitation pulses[10] were shown to function well under MAS, allowing the full spectral range of overtone signals to be excited in a single experiment. However, several observations went unexplained and appeared to be inconsistent with previous theoretical studies of MAS overtone NMR spectroscopy.[11–13] Most notably, the peak position under MAS showed a frequency shift relative to the static signal, exactly equal to twice the spinning frequency (ω_r). In addition to this, the other intense spinning sideband-like peaks at multiples of ω_r that were predicted by theory[12,13] appeared to be absent from the experimental spectra.

In this contribution, we report simulated ^{14}N MAS overtone NMR spectra generated using numerically exact calculations. These simulations accurately reproduce the observed experimental phenomena, providing an explanation for the (apparent) MAS rate-dependent frequency shift. We also present experimental spectra that demonstrate the potential of MAS overtone NMR to obtain high-resolution, information rich ^{14}N spectra directly from powder samples. In Sec. II, the relevant theory and simulation details are outlined. In Sec. III we describe the experimental methodology used to acquire the spectra, and in Sec. IV we compare the experimental results and simulations, discussing several interesting observations. Section V summarizes the main conclusions of this study.

II. THEORY AND SIMULATION DETAILS

In this section we describe the theory necessary to perform numerically exact simulations of overtone NMR under sample spinning conditions. The full time-dependent nuclear spin Hamiltonian of a single quadrupolar spin S in a static external field is given by

$$H(t) = H_Z + H_Q(t) + H_{CS}(t) + H_{rf}(t), \tag{1}$$

where

$$H_Z = -\gamma B_0 S_z = \omega_0 S_z \tag{2}$$

is the Hamiltonian of the Zeeman interaction of the S-spin nuclear magnetic moment with the static external magnetic field B_0 parallel to the z-axis and $\omega_0 = -\gamma B_0$ is the Larmor frequency of S.

$$H_Q(t) = \sum_{q=-2}^{2} (-1)^q \left[A_{2q}^Q(t)\right]^L T_{2-q}^Q \tag{3}$$

denotes the Hamiltonian of the quadrupolar interaction, where $[A_{2q}^Q(t)]^L$ is the component q of the irreducible 2nd rank quadrupolar tensor in the laboratory frame and T_{2-q}^Q is the component $-q$ of the 2nd rank irreducible spherical spin tensor. These components are given by $T_{20}^Q = \{3S_z^2 - S(S+1)\}/\sqrt{6}$, $T_{2\pm1}^Q = \mp\{S_z S^\pm + S^\pm S_z\}/2$, and $T_{2\pm2}^Q = S^\pm S^\pm/2$.

The component q of an irreducible 2nd rank interaction tensor Λ in the laboratory frame is, in general, obtained by transforming it from the principal axis system as follows:

$$\left[A_{2q}^\Lambda(t)\right]^L = \sum_{m'',m',m=-2}^{2} \left[A_{2m''}^\Lambda\right]^P D_{m''m'}^{(2)}\left(\Omega_{PM}^\Lambda\right) \times D_{m'm}^{(2)}(\Omega_{MR}) d_{mq}^{(2)}(-\theta_r) e^{im\omega_r t}. \tag{4}$$

The Euler angles $\Omega_{PM}^\Lambda = \{\alpha_{PM}^\Lambda, \beta_{PM}^\Lambda, \gamma_{PM}^\Lambda\}$ specify the relative orientation of the principal axis frame of the interaction and a molecular-fixed frame. The Euler angles $\Omega_{MR} = \{\alpha_{MR}, \beta_{MR}, \gamma_{MR}\}$ relate the molecular frame to a rotor-fixed frame and are random variables in a powder. Finally, the Euler angles $\Omega_{RL} = \{-\omega_r t, -\theta_r, 0\}$ describe the transformation of the rotor frame to the laboratory frame, where ω_r is the spinning frequency and θ_r is the angle between the rotor axis and the static external magnetic field.[14] For $\omega_r > 0$, the sample undergoes a right-handed rotation around the rotor axis, whereas for $\omega_r < 0$, the rotation is left-handed. A rotor angle of $\theta_r = \arctan\sqrt{2}$ (≈54.7°) corresponds to magic-angle spinning, for $\theta_r = 0$ and $\theta_r = \pi/2$ the sample is rotated around an axis parallel and orthogonal to the external field, respectively.

In case of the quadrupolar tensor, only the components $[A_{20}^Q]^P = \omega_Q/\sqrt{6}$ and $[A_{2\pm2}^Q]^P = -\eta_Q[A_{20}^Q]^P/\sqrt{6}$ are nonzero, where $\omega_Q = 6\pi C_Q/(2S(2S-1))$ is the quadrupolar frequency, $C_Q = eV_{33}Q/h$ is the quadrupolar coupling constant, and $\eta_Q = (V_{11} - V_{22})/V_{33}$ is the asymmetry parameter of the quadrupolar tensor. V_{11}, V_{22}, and V_{33} denote the principal components of the electric field gradient tensor labeled such that $|V_{33}| \geq |V_{22}| \geq |V_{11}|$.

The Hamiltonian of the chemical shift interaction is given by

$$H_{CS}(t) = \omega_0\delta_{iso}S_z + \left[A_{20}^{CS}(t)\right]^L T_{10}^{CS} - \frac{\sqrt{3}}{2}\left\{\left[A_{21}^{CS}(t)\right]^L T_{1-1}^{CS} + \left[A_{2-1}^{CS}(t)\right]^L T_{11}^{CS}\right\}, \tag{5}$$

where $\delta_{iso} = (\delta_{11} + \delta_{22} + \delta_{33})/3$ denotes the isotropic chemical shift. The principal components of the chemical shift tensor are labeled such that $|\delta_{33} - \delta_{iso}| \geq |\delta_{11} - \delta_{iso}| \geq |\delta_{22} - \delta_{iso}|$. $[A_{2q}^{CS}(t)]^L$ is the component q of the 2nd rank chemical shift anisotropy (CSA) tensor in the laboratory frame transformed from its principal axis system according to Eq. (4). In case of the CSA, only the components $[A_{20}^{CS}]^P = \omega_0\delta_{aniso}$ and $[A_{2\pm1}^{CS}]^P = -\eta_{CS}[A_{20}^{CS}]^P/\sqrt{6}$ are nonzero, where $\delta_{aniso} = \delta_{33} - \delta_{iso}$ is the anisotropic chemical deshielding constant and $\eta_{CS} = (\delta_{22} - \delta_{11})/\delta_{aniso}$ is the asymmetry

parameter. T_{1q}^{CS} is the component q of the 1st rank irreducible spherical spin tensor. These components are given by $T_{10}^{CS} = S_z$ and $T_{1\pm1}^{CS} = \mp S^{\pm}/\sqrt{2}$.

During a radiofrequency (rf) pulse, the total S-spin Hamiltonian is given by

$$H_{pulse}(t) = H(t) + H_{rf}(t), \tag{6}$$

where the Hamiltonian of the interaction of the S-spin nuclear magnetic moment with the oscillating magnetic field inside the rf coil, whose axis is collinear to the rotor spinning axis, is given by

$$H_{rf}(t) = \omega_{rf}(S_x \sin\theta_r + S_z \cos\theta_r)\cos(\omega_{ref} t + \phi_p) \tag{7}$$

with $\omega_{rf} = -\gamma B_{rf}$ and where B_{rf} is the amplitude of the oscillating magnetic field. The spectrometer reference frequency and rf phase are denoted ω_{ref} and ϕ_p, respectively. In the case of NMR spectroscopy at the fundamental Larmor frequency $\omega_{ref} \approx |\omega_0|$ is selected, whereas in overtone NMR $\omega_{ref} \approx |2\omega_0|$ is chosen.

The complete NMR signal (fundamental and overtone) may be calculated by propagating the equilibrium density matrix of the system of single quadrupolar spins employing (i) the propagator $U_{pulse}(t_p, t_0)$ during the rf pulse of duration $\tau_p = t_p - t_0$ and (ii) the propagator $U(t, t_p)$ during the acquisition of the complete NMR signal $s(t)$, where t_0 and t_p denote the time points at the start and the end of the pulse, respectively, and t indicates a general time point during signal acquisition:

$$s(t) = Tr[QU(t, t_p)U_{pulse}(t_p, t_0)\rho_{eq}U_{pulse}^{\dagger}(t_p, t_0)U^{\dagger}(t, t_p)], \tag{8}$$

where $\rho_{eq} = S_z$ is the equilibrium density matrix and Q is the detection operator

$$Q = S_x \sin\theta_r + S_z \cos\theta_r \tag{9}$$

for signal detection in the rf coil, whose axis is oriented collinear to the rotor spinning axis.

The propagator $U_{pulse}(t, t_0)$ solves the Schrödinger equation

$$\frac{d}{dt}U_{pulse}(t, t_0) = -i\,H_{pulse}(t)U_{pulse}(t, t_0) \tag{10}$$

with the initial condition $U_{pulse}(t_0, t_0) = 1$, and the propagator $U(t, t_p)$ solves the Schrödinger equation

$$\frac{d}{dt}U(t, t_p) = -i\,H(t)U(t, t_p) \tag{11}$$

with the initial condition $U(t_p, t_p) = 1$.

In this contribution, we calculate the overtone NMR signal of a single ^{14}N spin subsequent to a rf pulse at the overtone frequency using Mathematica[15] employing the SpinDynamica 2.5.3 code, programmed by Malcolm H. Levitt, available at http://www.spindynamica.soton.ac.uk. These simulations take the full nuclear spin Hamiltonian during the rf pulse Eq. (6) and during signal detection Eq. (1) into account. First, the propagator $U_{pulse}(t_p, t_0)$ is calculated by numerically solving the differential equation (10) using the matrix representation of the Hamiltonian and propagator, where ultimately the Mathematica routine `NDSolve` with its standard settings is employed.[15] For the case presented here, `NDSolve` employs the LSODA solver that automatically switches between the Adams-Bashforth method and the backward differentiation formulae (BDF) method,[16] where the size of the steps in the time dimension is adaptively adjusted.[15] This is a more general approach than the one used in popular software packages such as Simpson[17] and Spinevolution,[18] in which the interval $[t_0, t_p]$ is divided into small subintervals of equal length over which the Hamiltonian is assumed to be piecewise time-independent in order to be able to straightforwardly calculate the propagator over each subinterval via the matrix exponential. Second, the subsequent overtone NMR signal is calculated with the help of the COMPUTE algorithm,[19] during which the differential equation (11) is solved numerically. The number of points n chosen in one rotor period for the COMPUTE algorithm is adjusted to avoid spectral overlap of the spectrally folded fundamental and overtone NMR signals. The following parameter pairs were chosen for the simulations in this contribution: $(\omega_r/2\pi, n)$ = (10 kHz, 342), (22 kHz, 362), (50 kHz, 202), (70 kHz, 146). We modified the SpinDynamica code to enable powder averaging using 6044 triplets of Euler angles, selected according to the ZCW scheme,[20] utilizing multiple processor cores in parallel. Examples of the Mathematica code used for these calculations are given in the supplementary information.[21]

All numerical simulations are performed at a ^{14}N fundamental Larmor frequency of 36 MHz, i.e., an overtone frequency of 72 MHz. To match the simulated rf values to the experiments, the rf nutation frequency of the fundamental ^{2}H resonance in liquid D_2O, $\omega_{rf}^{^2H}/2\pi$, was measured and converted according to

$$\omega_{rf}^{^{14}N} = \frac{\gamma^{^{14}N}}{\gamma^{^2H}} \frac{2}{\sin(\arctan\sqrt{2})} \omega_{rf}^{^2H}, \tag{12}$$

where the second factor represents the scaling due to the orientation of the rf coil at the magic-angle with respect to the external field and the transformation into the rotating rf frame in case of the ^{2}H nuclei.

III. EXPERIMENTAL DETAILS

All ^{14}N MAS overtone NMR spectra in this study were obtained at a magnetic field strength of 11.7 T on a Bruker Avance III 500 spectrometer. This field corresponds to a ^{14}N overtone resonance frequency of 72.3 MHz. Spectra were recorded using single-pulse excitation. As mentioned above, the rf powers specified for each sample below were determined from the nutation frequency of the fundamental ^{2}H transition in D_2O (which is close in frequency to the ^{14}N overtone transition) using Eq. (12). All spectra are referenced such that 0 kHz corresponds to twice the absolute frequency of the (fundamental) ^{14}N NMR signal obtained from solid NH_4Cl. Samples were purchased from Sigma Aldrich and used without further alteration, and experimental spectra were processed using the NUTS software (Acorn NMR).

The ^{14}N MAS overtone NMR spectrum of glycine was acquired with a 4.0 mm Varian T3 probe, a MAS rate of 10 kHz, and a rf field strength of $\omega_{rf}^{^{14}N}/2\pi = 48.4$ kHz. A total of 10 000 scans were acquired using a standard (fixed-frequency) pulse 100 μs in length and applied

on-resonance with the observed signal. The recycle delay was 0.5 s. For L-proline, a 3.2 mm Varian T3 probe and MAS rate of 20 kHz were used. About 200 000 scans were acquired using a standard 50 μs on-resonance pulse with a rf field strength of $\omega_{rf}^{^{14}N}/2\pi = 80.7$ kHz and a recycle delay of 0.5 s. Continuous-wave ^{1}H decoupling was applied for both glycine and proline ($\nu_1 = 80$ kHz), and a pre-acquisition delay (dead-time) of 50 μs was used to minimize the effects of acoustic probe ringing.

The L-histidine spectrum was acquired at a MAS rate of 22 kHz with a 3.2 mm Varian T3 probe. A total of 65 000 scans were acquired with a recycle delay of 4 s. For this sample, a WURST-80 excitation pulse[10] was used with a pulse length of 100 μs, a total frequency sweep range of 150 kHz (centered at 60 kHz on the spectrum's frequency scale), and a maximum rf field strength of $\omega_{rf}^{^{14}N}/2\pi = 80.7$ kHz. The pulse shape was generated using the Bruker ShapeTool software and was applied with CYCLOPS phase cycling. XiX ^{1}H decoupling[22] was also used with $\nu_1 = 80$ kHz and a pulse length of 129.5 μs. Due to the phase dispersion in the acquired signal imparted by the WURST excitation pulse, a second-order phase correction was applied to the spectrum after Fourier transformation.[23]

In addition to the ^{14}N MAS overtone NMR, two additional experiments were carried out on L-histidine as an independent means of measuring the isotropic shift and quadrupolar parameters for the various nitrogen sites. A natural abundance ^{15}N CPMAS spectrum was acquired at 11.7 T at a MAS rate of 10 kHz and a 2 ms contact time, with 4000 scans acquired and a recycle delay of 5 s. The ^{14}N ultra-wideline spectrum was recorded at 21.1 T using the WURST-QCPMG pulse sequence[24] and a piecewise acquisition method described in detail in Ref. 25. Nine sub-spectra were acquired, each with 800 scans and a recycle delay of 4 s.

The ^{14}N NMR interaction parameters for L-histidine were also calculated from the known crystal structure[26] using density functional theory, specifically the CASTEP software.[27] Perdew, Burke, and Ernzerhof functionals were used with a plane wave basis set cutoff of 610 eV and a 3 × 2 × 1 Monkhorst-Pack k-space grid. Hydrogen atom positions were optimized prior to the calculation of the NMR parameters. Calculated isotropic shielding values for ^{14}N were converted to isotropic chemical shifts using a previously reported formula.[25] These isotropic chemical shifts are reported relative to the fundamental ^{14}N NMR signal from solid NH_4Cl at 0 ppm. Calculated values for the Euler angles were extracted from the CASTEP output files using the EFGShield software.[28] The experimental and calculated ^{14}N NMR parameters for this sample are summarized in Table I, including quadrupolar parameters for site N3 previously measured using NQR.[29] Experimental and calculated ^{14}N parameters for glycine and L-proline are reported in Refs. 25 and 30.

TABLE I. Experimental (bold type) and calculated (regular type) ^{14}N NMR parameters for L-histidine (orthorhombic phase).

Site	C_Q (MHz)	η_Q	δ_{iso} (ppm)	δ_{aniso} (ppm)	η_{CS}	α (°)	β (°)	γ (°)
N1	1.30	0.07	8	10.2	0.92	99	13	325
	1.22[a]	**0.15**[a]	**2**[b]	…	…	…	…	…
N2	−3.46	0.07	221	−237	0.38	3	89	96
	3.30[a]	**0.12**[a]	**211**[b]	…	…	…	…	…
N3	−1.42	0.98	151	−120	0.67	105	1	272
	1.44[c]	**0.92**[c]	**132**[b]	…	…	…	…	…

[a]Measured using ultra-wideline ^{14}N NMR at 21.1 T (this work).
[b]Measured using ^{15}N CPMAS NMR at 11.7 T (this work).
[c]Previously reported NQR values, see Ref. 29.

IV. RESULTS AND DISCUSSION

A. MAS overtone NMR spectra

The ^{14}N overtone NMR spectrum from a single nitrogen site at a fixed orientation with respect to the magnetic field shows a single peak at approximately twice the Larmor frequency, its exact position relative to this being determined by both the isotropic chemical shift and second-order quadrupolar shift. An example of such a spectrum can be seen in Figure 1(a), simulated for a stationary single crystal of glycine at 11.7 T. When the effects of MAS are included in the simulation (Figure 1(b)), the signal is split into five sidebands with different phases and intensities, and relative shifts of 0, $\pm\omega_r$, and $\pm 2\omega_r$ as predicted by a previous theoretical treatment.[12] These overtone sidebands are fundamentally

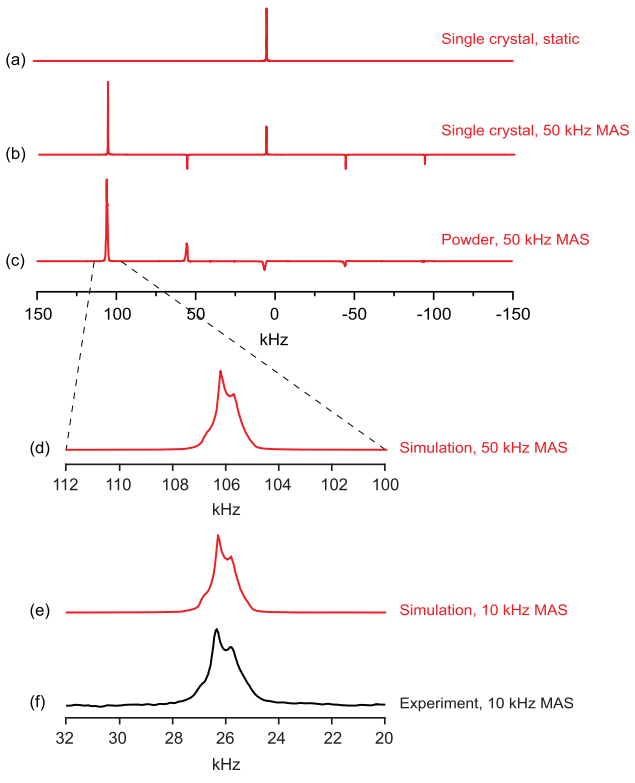

FIG. 1. Numerically exact simulations of ^{14}N overtone spectra for (a) a single crystal of glycine at an arbitrary orientation, (b) the same single crystal under 50 kHz MAS, and (c) glycine powder spinning at 50 kHz MAS. Parameters used in the simulations are $\delta_{iso} = -6$ ppm, $C_Q = 1.18$ MHz, and $\eta_Q = 0.53$, and the simulated pulse length and ^{14}N rf field strength were 0.1 μs and 161.5 kHz, respectively. An expansion of the $+2\omega_r$ sideband taken from the 50 kHz MAS simulation is shown in (d), and from a 10 kHz MAS simulation with a pulse length and ^{14}N rf field strength of 100 μs and 48.4 kHz, respectively, in (e). The experimental spectrum obtained at 10 kHz MAS is shown in (f).

different from conventional spinning sidebands that stem from the modulation of the spin interactions during sample rotation. The relative amplitudes of conventional sidebands due to *rotor-modulation* depend on the size of the spin interaction and the spinning frequency. These five overtone sidebands on the other hand stem from the orientational dependence, hence rotor-position dependence, of the detection of the overtone signal, therefore they may be compared to sidebands due to *rotor-encoding* in double-quantum spectroscopy.[31] The relative amplitudes of the rotor-encoding overtone sidebands are independent of the spinning frequency (i.e., they will remain present at all MAS rates). Since the detection of the overtone signal is enabled by the second rank quadrupolar interaction, a total of five rotor-encoded overtone sidebands are observed.

In order to account for all possible crystallite orientations present within a powder sample, the simulation in Figure 1(b) was repeated for a set of 6044 orientations to produce the powder MAS overtone NMR spectrum (Figure 1(c)). In this case, the $+2\omega_r$ sideband is prominent, while the other sidebands show a much lower intensity. Spinning at the magic angle, therefore, results in this $+2\omega_r$ overtone sideband being preferentially selected, while the signals from the centreband and other sidebands are much weaker (the $+\omega_r$ sideband shows ~10% of the signal intensity of the $+2\omega_r$ sideband, and the others even less). This provides an explanation for the (apparent) frequency shift of $+2\omega_r$ that was previously observed for ^{14}N overtone NMR spectra under MAS.[9] Figure 1(d) shows an expanded view of the $+2\omega_r$ sideband. A powder pattern with several sharp features and shoulders is visible that is similar (but not identical) in shape to the second-order quadrupolar powder patterns observed from central transitions of half-integer quadrupolar nuclei under MAS.

The simulations discussed thus far were carried out with short (0.1 μs) rf pulses to provide uniform excitation across the full overtone frequency range and a fast MAS rate of 50 kHz to facilitate shorter calculation times. Figure 1(e) instead shows a simulation accounting for the exact experimental conditions used (i.e., 10 kHz MAS with a 100 μs pulse applied on resonance with the $+2\omega_r$ sideband). This powder pattern matches remarkably well in shape, size, and position with the experimental spectrum in Figure 1(f). We note that this is the first time that a simulated MAS overtone NMR spectrum has been matched to experimental results and the agreement is excellent. We also note that the powder patterns exhibited by the $+2\omega_r$ sideband in both simulations line up exactly if the 50 kHz MAS simulation is shifted by -80 kHz (i.e., twice the difference in simulated spinning rates). This shows that faster MAS rates can safely be used to speed up the calculation times in these numerically exact simulations provided that the rate difference is subsequently accounted for by such a shift.

In previous work[9] O'Dell and Ratcliffe reported an apparent absence of other spinning sidebands in the MAS overtone spectrum of glycine. Our simulations now allow us to attribute this observation to the narrow bandwidth of the 100 μs excitation pulse used. Figure 2(a) shows an expanded view of the glycine simulation accounting for the exact experimental conditions, and this can be compared

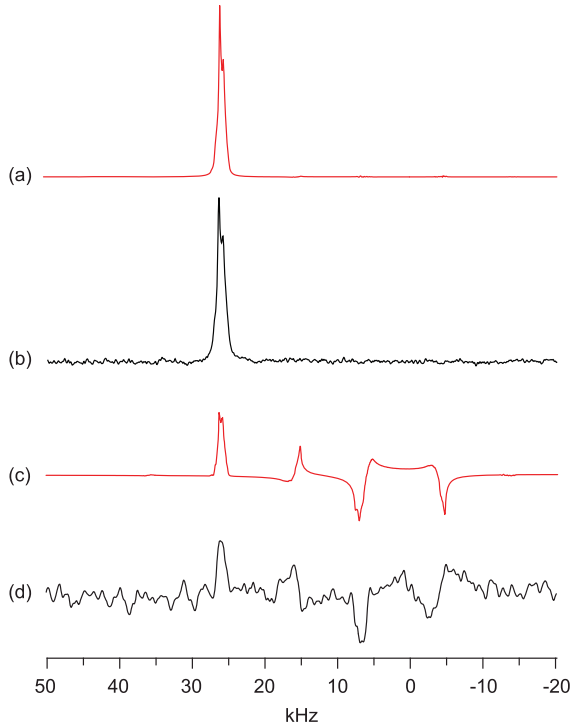

FIG. 2. ^{14}N overtone NMR spectra obtained from a powder sample of glycine at 11.7 T and 10 kHz MAS. Spectrum (a) was obtained with a 100 μs pulse applied on-resonance with the observed signal and 10 000 scans acquired. Spectrum (c) was obtained with a 50 μs pulse applied at an offset of -20 kHz (i.e., at the position of the overtone centreband) with 400 000 scans acquired. Numerically exact simulations of these experimental conditions are shown in (b) and (d). Only zero-order phasing was applied to the simulation in (d) to match with the experiment.

to the experimental spectrum in Figure 2(b) in which the other overtone sidebands and centreband are absent. In this case, these latter features lie outside of the excitation bandwidth of this relatively long rf pulse. Figures 2(c) and 2(d) show that the other overtone sidebands can be observed experimentally under certain conditions, albeit with a significantly lower signal intensities. In these spectra, a 50 μs pulse was applied at the position of the centreband, corresponding to an ~180° nutation angle for the $+2\omega_r$ sideband as shown previously (see Figure 2 in Ref. 9). After 400 000 scans, the centreband is visible, as are the sidebands at $+\omega_r$ and $-\omega_r$. The $+2\omega_r$ sideband also shows some small intensity due to the nutation angle not being exactly 180° for that peak. The sideband at $-2\omega_r$ is not visible above the level of the noise and is also absent in the simulation. Since the spectrum in Figure 2(b) was obtained in just 10 000 scans, this provides an experimental confirmation of the very low signal intensity present in the overtone centreband and $\pm\omega_r$ sidebands compared with that of the main $+2\omega_r$ sideband when correctly excited.

The simulations in Figure 3 provide an illustration of typical MAS NMR powder patterns exhibited by the $+2\omega_r$ overtone sideband. As the asymmetry parameter η_Q is increased, the two sharp features visible in the $\eta_Q = 0.0$ powder pattern are seen to converge and meet at $\eta_Q = 1.0$ in a fashion that is analogous to central transition MAS powder patterns of half-integer quadrupolar nuclei. The centre of gravity of

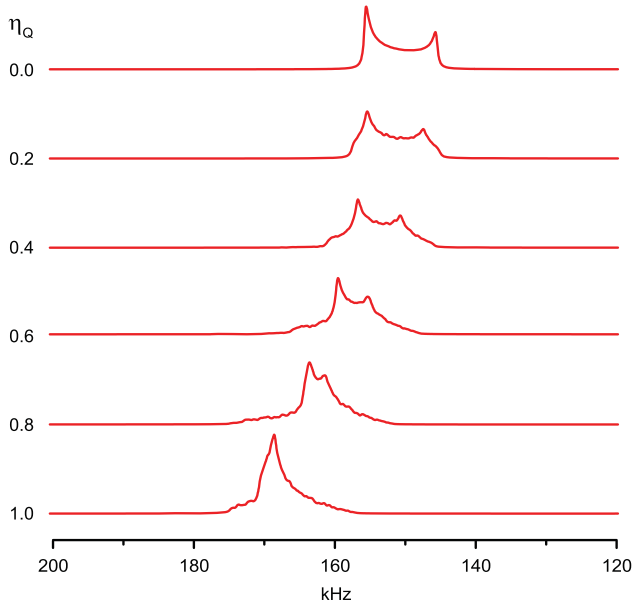

FIG. 3. Simulated ^{14}N overtone MAS powder patterns ($+2\omega_r$ sidebands) for a nitrogen site with $\delta_{iso} = 0$ ppm, $C_Q = 3.5$ MHz, and the η_Q values shown at 11.7 T and a MAS rate of 50 kHz. The simulated rf pulses were 0.2 μs in length with $\omega_{rf}^{^{14}N}/2\pi = 161.5$kHz.

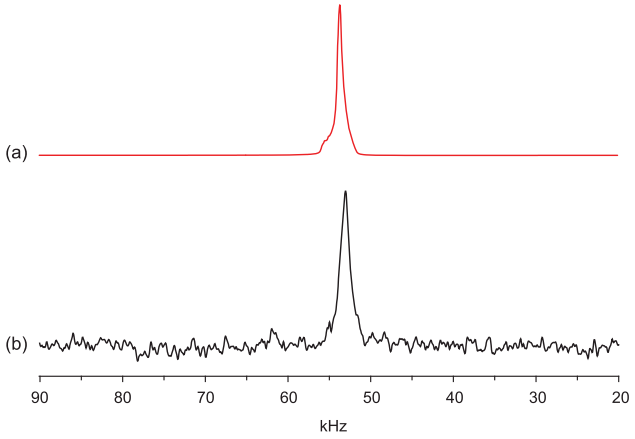

FIG. 4. Simulated (a) and experimental (b) ^{14}N overtone MAS NMR spectrum of L-proline at 11.7 T. The experimental spectrum was obtained at a MAS rate of 20 kHz. The simulated spectrum was made with parameters $\delta_{iso} = 24$ ppm, $C_Q = 1.47$ MHz, and $\eta_Q = 0.98$. The MAS rate was specified as 70 kHz and the simulation was then shifted by −100 kHz. The simulated rf pulse was 0.2 μs in length with $\omega_{rf}^{^{14}N}/2\pi = 161.5$kHz.

the powder pattern also moves to a higher frequency as η_Q is increased. The width of these powder patterns increases with the size of the quadrupolar interaction (proportional to ω_Q^2/ω_0, see supplementary information[21]), while their positions are determined by both the isotropic shift δ_{iso} and second-order quadrupolar shift δ_Q. Due to the overtone signal originating from the $\Delta m = 2$ transition, the position of the powder pattern is, in fact, twice as sensitive to the isotropic chemical shift (in terms of absolute frequency) than the signal arising from the fundamental transitions.

Experimental overtone MAS powder patterns can, therefore, be simulated to extract three distinct ^{14}N NMR parameters (δ_{iso}, C_Q, and η_Q), making them also analogous to central transition MAS powder patterns of half-integer quadrupolar nuclei in terms of information content. We note that the ^{15}N CPMAS spectrum is dependent only on δ_{iso}, making this a potentially useful complementary method that can provide a constraint on the fitting of the MAS overtone spectrum. The quadrupolar parameters C_Q and η_Q can also, in principle, be measured from ^{14}N spectra obtained indirectly via two-dimensional HMQC-type experiments, though in practice such indirectly observed ^{14}N powder patterns tend to be distorted away from their ideal simulated shapes.[2] As an additional example, the experimental and simulated ^{14}N MAS overtone spectra of L-proline ($\eta_Q = 0.98$) are shown in Figure 4.

B. Dependence on spinning angle and sense

The simulations in Figures 5(a) and 5(b) illustrate the difference between static and MAS overtone powder patterns. The static powder pattern for glycine shows a broad feature that tails off on the low frequency side, and covers a frequency range of ∼5 kHz at 11.7 T. Under MAS, the $+2\omega_r$ overtone sideband has a similar width at half height as the static pattern (∼1 kHz) but a much reduced width at its base (around 2 kHz). For many nitrogen sites, the static overtone powder pattern will be further broadened by the CSA, an interaction that can be averaged away completely by MAS. ^{14}N MAS overtone NMR, therefore, provides significant advantages in terms of line-narrowing and increased resolution over experiments on static samples, as has previously been shown.[9] This is discussed further in Sec. IV C.

Frydman and co-workers carried out a theoretical treatment of sample spinning in overtone NMR spectroscopy, simulating spectra spinning at various angles relative to the magnetic field using perturbation theory and rotating frame transformations.[12] They concluded that the characteristics of the spectra were highly sensitive to the spinning angle. In particular, for the case of a sample spinning about an axis parallel to the magnetic field, the spectrum was predicted to be identical in shape to the static powder pattern but shifted by ω_r. The authors offered a qualitative explanation for this phenomenon in terms of the time dependence imposed on the rotating frame by the sample spinning. However, their simulations, as well as those shown in Refs. 11 and 13 do not match with the experimental results we have obtained, indicating that their theoretical treatment is incomplete. Although perturbation approaches or similar approximations can, in principal, allow a more understandable physical insight into the phenomena under study (as well as faster and more efficient calculation of spectra), the results must first be matched to experiments to demonstrate their validity. Our exact numerical treatment on the other hand is a "black box" approach, but does reproduce all of our observed experimental results extremely accurately. We expect that an improved perturbation treatment will provide a far better means of simulating these experiments, but this is beyond the scope of this article.

Our numerically exact simulations show that for a sample spinning about an axis parallel to the magnetic field, solely the

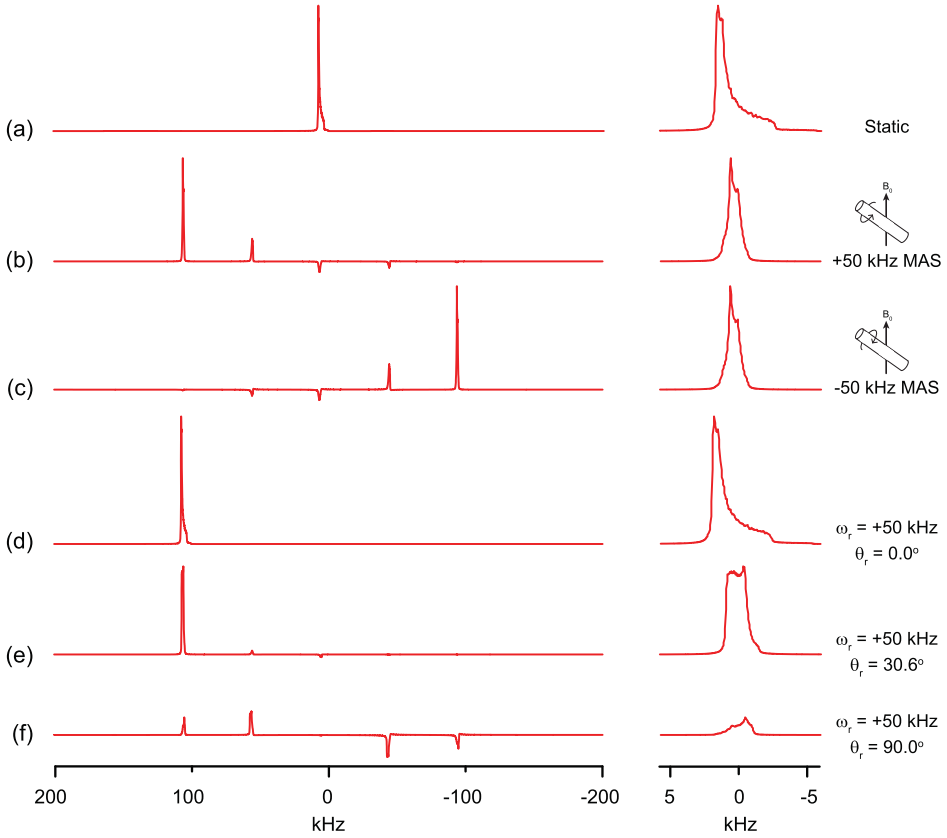

FIG. 5. Simulated ^{14}N overtone NMR spectra for glycine (powder) at 11.7 T under (a) static conditions, (b) +50 kHz MAS, (c) −50 kHz MAS (spinning directions as shown), and 50 kHz spinning about an axis oriented at an angle of (d) 0, (e) 30.6, and (f) 90° relative to the magnetic field. Specific regions are shown on the right with an expanded horizontal scale showing the $+2\omega_r$ sidebands. The simulated rf pulse lengths were 0.1 μs with $\omega_{rf}^{14N}/2\pi = 161.5$ kHz.

$+2\omega_r$ overtone sideband is present in the overtone spectrum, retaining the same shape as the static powder pattern. Hence, the signal *appears* to be shifted by $2\omega_r$ (Figures 5(a) and 5(d)). Spinning the sample at other angles results in changes to the shape of the $+2\omega_r$ overtone sideband, as well as differences in relative signal intensity for the other overtone sidebands. For example, spinning the sample perpendicular to the magnetic field results in the $\pm\omega_r$ sidebands showing a greater intensity than the $\pm2\omega_r$ sidebands, while the centreband is absent (Figure 5(f)). Spinning the sample at the magic angle, however, provides the additional benefit of averaging the CSA and heteronuclear dipolar couplings, making this angle the most useful for practical purposes, although it remains possible that two-dimensional DAS-style experiments[32] in which the spinning axis is rapidly switched between angles could lead to advantages such as the complete removal of the anisotropic quadrupolar broadening.

Due to the preferred selection of the $+2\omega_r$ overtone sideband, the MAS overtone spectrum is also dependent on the sense of the spinning. If the spinning direction is reversed (i.e., becomes negative), it is still the $+2\omega_r$ sideband that is preferentially selected, with the powder pattern retaining the same shape and orientation, but the negative spinning rate now causes this sideband to appear on the opposite side with a negative frequency shift relative to the static pattern (Figure 5(c)). Such a dependence of the NMR spectrum on the spinning sense is extremely uncommon in solid-state NMR. Spinning sideband manifolds from single-crystal or preferentially oriented samples can show differences that depend on the spinning sense, but generally in solid-state NMR of powders the presence of all possible crystallite orientations is sufficient to average out these effects, as has been demonstrated for the case of a spin-1/2 nucleus experiencing a CSA.[33]

C. Resolution of the three nitrogen sites in L-histidine

The amino acid L-histidine has three distinct nitrogen environments in its crystalline (orthorhombic) form (Figure 6(a)), and these have been characterized previously using indirectly detected ^{14}N NMR methods[34] as well as ^{14}N NQR.[29] The nitrogen NMR parameters calculated from the crystal structure using DFT are presented in Table I, along with some experimental values for δ_{iso}, C_Q, and η_Q. The isotropic chemical shifts were determined from the ^{15}N CPMAS spectrum shown in Figure 6(b). Two observations can be made about this spectrum. First, the signal intensity for the N2 peak is lower than that of the others due to the N2 site lacking a directly bonded hydrogen, resulting in less efficient ^{1}H to ^{15}N cross-polarization. Second, the N3 peak is broader than those of N1 and N2, suggesting that the magnetization from this site experiences a faster transverse relaxation. This latter fact is important in the interpretation of the ultra-wideline NMR spectrum obtained from the fundamental ^{14}N transitions at 21.1 T (Figure 6(c)), in which only

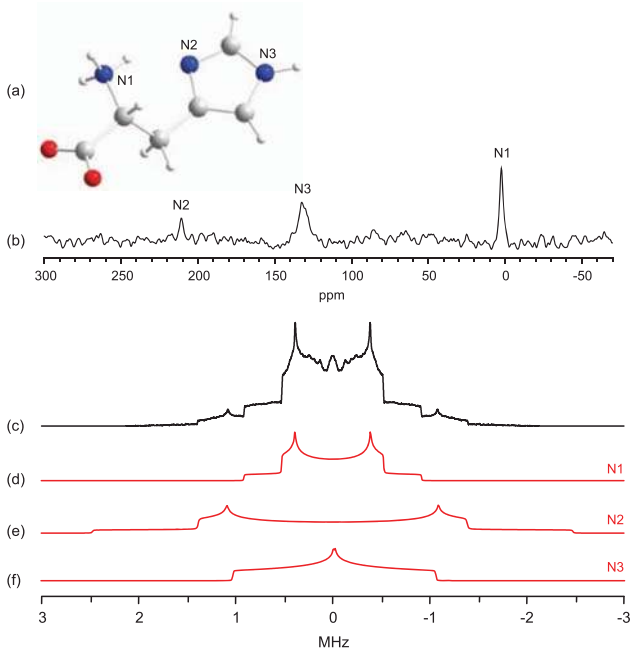

FIG. 6. (a) Molecular structure of L-histidine with the nitrogen sites labeled. (b) Experimental ^{15}N CPMAS spectrum of L-histidine (orthorhombic phase) at 11.7 T and 10 kHz MAS. (c) Experimental ^{14}N ultra-wideline (fundamental) spectrum of a static powder sample of L-histidine obtained at 21.1 T. Simulations of the ultra-wideline ^{14}N powder patterns for the three individual nitrogen sites are shown in (d), (e), and (f).

the powder patterns from sites N1 and N2 can be clearly observed. This spectrum was acquired using the WURST-QCPMG pulse sequence,[24] for which the effects of transverse relaxation have been shown to result in the selective signal enhancement of more slowly relaxing nitrogen sites.[25] For the purposes of the ^{14}N MAS overtone simulations, C_Q and η_Q values reported in a NQR study[29] were, therefore, used for site N3, while values determined from the ultra-wideline NMR spectrum in Figure 6(c) were used for N1 and N2 (Table I).

Simulated ^{14}N overtone NMR spectra of L-histidine are shown in Figures 7(a) and 7(b) for a static powder sample, neglecting and including the effects of the CSA, respectively. Site N2 has a very large CSA (spanning 400 ppm or 30 kHz for the ^{14}N overtone transition at 11.7 T), and this can be seen to broaden the static overtone powder pattern significantly (Figure 7(b)). Such a broad pattern would be very difficult to obtain experimentally using single-pulse excitation due to the pre-acquisition delay (particularly with a WURST pulse). Under MAS, the simulations with and without CSA look almost identical (Figures 7(c) and 7(d)), demonstrating that MAS averages away the effects of the CSA in overtone experiments as one would expect. All three powder patterns are narrowed by MAS, and in particular the pattern width for site N2 is reduced by approximately a factor of 4. The intensity of the $+\omega_r$ overtone sideband arising from site N2 also appears in these MAS simulations with a relatively high intensity (marked in the figure by the asterisks). We attribute this to the very short pulse duration of 0.2 μs used in these simulations, and have found that longer simulated pulse lengths, e.g., 1 μs lead to a more intense $+2\omega_r$ sideband compared to $+\omega_r$. We were not able to obtain experimental spectra for very short pulse durations, however, as the overall signal to noise ratio is very low in this case. Hence, we found it difficult to experimentally observe sidebands other than the $+2\omega_r$ sideband.

The experimental spectrum is shown in Figure 7(f). This spectrum was obtained with a WURST excitation pulse, which provides broadband excitation even under MAS as we have previously shown.[9] Figure 7(e) shows a simulation calculated for the exact experimental parameters used, and the agreement is excellent for all three sites, with even the individual powder pattern shapes for each site matching up to a good degree of accuracy. The $+\omega_r$ overtone sideband from site N2, which was relatively intense in the 70 kHz MAS simulations, is absent in both of these spectra (note that due to the slower experimental MAS rate, this sideband would be expected to appear in the experimental spectrum approximately half-way between the N2 and N3 peaks, yet is not visible above the level of the noise). As well as the much longer pulse length, this may be a result of the frequency-swept nature of the WURST excitation pulse, and we are currently investigating this in more detail.

The ^{14}N MAS overtone powder patterns for the three nitrogen sites are, therefore, extremely well resolved at 11.7 T, and the advantages of this approach over ultra-wideline methods (Figure 6(c)) in terms of both resolution and spectral width are readily apparent. The overtone spectrum also shows a higher level of information content than either the fundamental ^{14}N spectrum or the ^{15}N CPMAS spectrum, providing not only the isotropic chemical shifts but also quantitative information on the quadrupolar interaction tensors for each site, which are highly sensitive to the local structural environment (e.g., hydrogen bonding arrangements).[25] MAS overtone NMR spectroscopy, therefore, provides a relatively straightforward means of acquiring high-resolution ^{14}N NMR spectra directly from powder samples. The main disadvantage of this approach is its relatively low sensitivity, the spectrum in Figure 7(e) having taken 3 days of experimental time to acquire and still showing a relatively low signal to noise ratio. This factor must be addressed if this approach is to become a routine experiment. We are currently investigating a number of methodological improvements to address this issue, including the possibility of cross-polarization from ^{1}H nuclei directly to the overtone transition, which has already been demonstrated on static samples.[8]

V. SUMMARY

Numerically exact simulations of ^{14}N overtone NMR spectra under magic angle spinning conditions result in spectra that agree extremely well with experimental results. MAS causes the preferential selection of a single spinning sideband at $+2\omega_r$ of a set of five (0, $\pm$1, $\pm$2) overtone sidebands, resulting in a corresponding apparent shift to high or low frequency depending on the sense of spinning. The other overtone sidebands and centreband are much lower in intensity, but can be observed experimentally. MAS also averages the effects of chemical shielding anisotropy, resulting in significant narrowing of the powder pattern linewidths. The powder patterns show characteristic lineshapes from which the

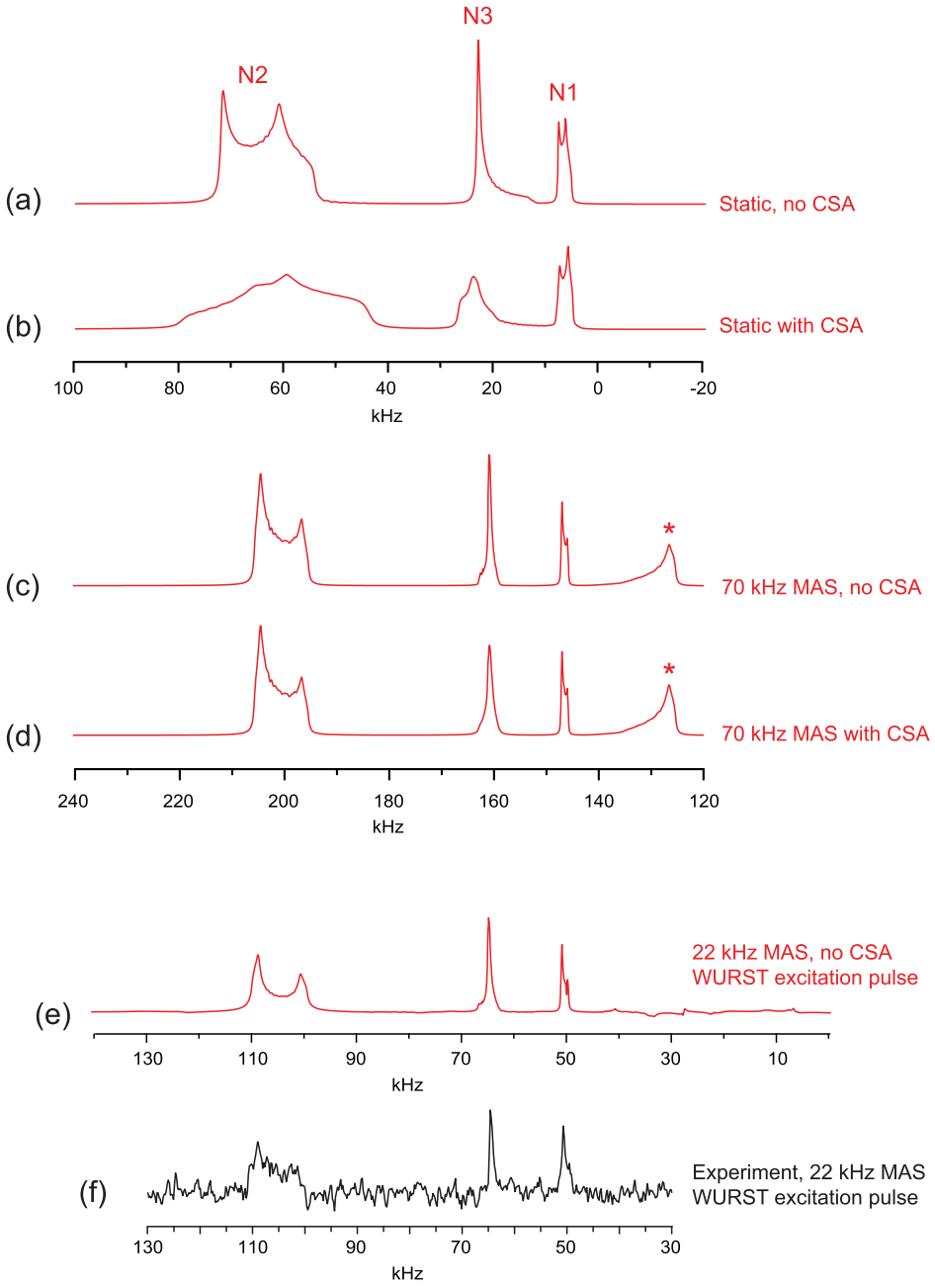

FIG. 7. Simulated ^{14}N overtone NMR spectra of L-histidine (orthorhombic phase) at 11.7 T (a) static without effects of shielding anisotropy, (b) static including shielding anisotropy, (c) 70 kHz MAS without shielding anisotropy, and (d) 70 kHz MAS with shielding anisotropy. Parameters used in the simulations are shown in Table I. Asterisks denote $+\omega_r$ sidebands arising from site N2. Simulations (a) to (d) were made using short pulses to ensure uniform excitation. The simulation in (e) was calculated for a 22 kHz MAS rate, neglecting the CSA but including the effects of a WURST excitation pulse matching the exact experimental conditions used to acquire the spectrum in (f). Simulated rf pulse lengths were 0.005 μs for (a) and (b), 0.2 μs for (c) and (d), and 100 μs (WURST-80, 150 kHz sweep range) for (e) with $\omega_{rf}^{^{14}\mathrm{N}}/2\pi = 80.7$ kHz.

quadrupolar parameters and isotropic shifts can be measured. The MAS overtone experiment, therefore, provides a straightforward method for the direct acquisition of high resolution ^{14}N NMR spectra from powder samples, as we have demonstrated for L-histidine.

ACKNOWLEDGMENTS

The authors would like to thank Victor Terskikh for help in acquiring the ultra-wideline ^{14}N NMR spectrum of L-histidine, and Malcolm H. Levitt and Michael C. D. Tayler for help with SpinDynamica. Access to the 21.1 T spectrometer was provided by the National Ultrahigh Field NMR Facility for Solids (Ottawa, Canada), a national research facility funded by the Canada Foundation for Innovation, the Ontario Innovation Trust, Recherche Québec, the National Research Council Canada, and Bruker BioSpin and managed by the University of Ottawa (http://www.nmr900.ca).

[1]L. A. O'Dell, Prog. Nucl. Magn. Reson. Spectrosc. **59**, 295 (2011).
[2]S. Cavadini, Prog. Nucl. Magn. Reson. Spectrosc. **56**, 46 (2010).

[3]H. J. Jakobsen, H. Bildsøe, J. Skibsted, and T. Giavani, J. Am. Chem. Soc. **123**, 5098 (2001).
[4]E. A. Hill and J. P. Yesinowski, J. Am. Chem. Soc. **118**, 6798 (1996).
[5]L. A. O'Dell and R. W. Schurko, J. Am. Chem. Soc. **131**, 6658 (2009).
[6]M. Bloom and M. A. LeGros, Can. J. Phys. **64**, 1522 (1986).
[7]R. Tycko and S. J. Opella, J. Am. Chem. Soc. **108**, 3531 (1986).
[8]R. Tycko and S. J. Opella, J. Chem. Phys. **86**, 1761 (1987).
[9]L. A. O'Dell and C. I. Ratcliffe, Chem. Phys. Lett. **514**, 168 (2011).
[10]E. Kupče and R. J. Freeman, J. Mag. Reson. A **115**, 273 (1995).
[11]K. Takegoshi and K. Hikichi, Chem. Phys. Lett. **194**, 359 (1992).
[12]L. Marinelli, S. Wi, and L. Frydman, J. Chem. Phys. **110**, 3100 (1999).
[13]N. M. Trease and P. J. Grandinetti, J. Chem. Phys. **128**, 052318 (2008).
[14]M. Ernst, J. Magn. Reson. **162**, 1 (2003).
[15]Wolfram Research, Inc., Mathematica, Version 8.0, Champaign, IL, 2011.
[16]A. C. Hindmarsh, "ODEPACK, A systematized collection of ODE solvers," in *Scientific Computing*, IMACS Transactions on Scientific Computation Vol. 1, edited by R. S. Stepleman *et al.* (North-Holland, Amsterdam, 1983), pp. 55–64.
[17]M. Bak and N. C. Nielsen, J. Magn. Reson. **147**, 296 (2000).
[18]M. Veshtort and R. G. Griffin, J. Magn. Reson. **178**, 248 (2006).
[19]M. Edén, Y. K. Lee, and M. H. Levitt, J. Magn. Reson. A **120**, 56 (1996).
[20]H. Conroy, J. Chem. Phys. **47**, 5307 (1967).
[21]See supplementary material at http://dx.doi.org/10.1063/1.4775592 for additional simulations and Mathematica notebook to calculate MAS overtone spectra.
[22]A. Detken, E. H. Hardy, M. Ernst, and B. H. Meier, Chem. Phys. Lett. **356**, 298 (2002).
[23]I. Hung and Z. Gan, J. Magn. Reson. **204**, 256 (2010).
[24]L. A. O'Dell and R. W. Schurko, Chem. Phys. Lett. **464**, 97 (2008).
[25]L. A. O'Dell, R. W. Schurko, K. J. Harris, J. Autschbach, and C. I. Ratcliffe, J. Am. Chem. Soc. **133**, 527 (2011).
[26]J. J. Madden, E. L. McGandy, and N. C. Seeman, Acta Crystallogr., Sect. B **28**, 2377 (1972).
[27]S. J. Clark, M. D. Segall, C. J. Pickard, P. J. Hasnip, M. J. Probert, K. Refson, and M. C. Payne, Z. Kristallogr. **220**, 567 (2005).
[28]S. Adiga, D. Aebi, and D. L. Bryce, Can. J. Chem. **85**, 496 (2007).
[29]M. J. Hunt, A. L. Mackay, and D. T. Edmonds, Chem. Phys. Lett. **34**, 473 (1975).
[30]L. A. O'Dell and R. W. Schurko, Phys. Chem. Chem. Phys. **11**, 7069 (2009).
[31]I. Schnell, Prog. Nucl. Magn. Reson. Spectrosc. **45**, 145 (2004).
[32]A. Llor and J. Virlet, Chem. Phys. Lett. **152**, 248 (1988).
[33]S. C. Shekar, Magn. Reson. Chem. **36**, 496 (1998).
[34]V. Vizthum, M. A. Caporini, S. Ulzega, and G. Bodenhausen, J. Magn. Reson. **212**, 234 (2011).